Alzheimer's Research & Therapy

RESEARCH

Open Access

Association of Alzheimer's disease polygenic risk scores with amyloid accumulation in cognitively intact older adults

Emma S. Luckett[1,2,3], Yasmina Abakkouy[3], Mariska Reinartz[1,2], Katarzyna Adamczuk[1,4], Jolien Schaeverbeke[1,2], Sare Verstockt[5], Steffi De Meyer[1,2,6], Koen Van Laere[7,8], Patrick Dupont[1,2], Isabelle Cleynen[3†] and Rik Vandenberghe[1,2,9*†]

Abstract

Background: Early detection of individuals at risk for Alzheimer's disease (AD) is highly important. Amyloid accumulation is an early pathological AD event, but the genetic association with known AD risk variants beyond the *APOE4* effect is largely unknown. We investigated the association between different AD polygenic risk scores (PRS) and amyloid accumulation in the Flemish Prevent AD Cohort KU Leuven (F-PACK).

Methods: We calculated PRS with and without the *APOE* region in 90 cognitively healthy F-PACK participants (baseline age 67.8 (52–80) years, 41 *APOE4* carriers), with baseline and follow-up amyloid-PET (time interval 6.1 (3.4–10.9) years). Individuals were genotyped using Illumina GSA and imputed. PRS were calculated using three *p*-value thresholds (pT) for variant inclusion: 5×10^{-8}, 1×10^{-5}, and 0.1, based on the stage 1 summary statistics from Kunkle et al. (Nat Genet 51:414–30, 2019). Linear regression models determined if these PRS predicted amyloid accumulation.

Results: A score based on PRS excluding the *APOE* region at $pT = 5 \times 10^{-8}$ plus the weighted sum of the two major *APOE* variants (rs429358 and rs7412) was significantly associated with amyloid accumulation ($p = 0.0126$). The two major *APOE* variants were also significantly associated with amyloid accumulation ($p = 0.0496$). The other PRS were not significant.

Conclusions: Specific PRS are associated with amyloid accumulation in the asymptomatic phase of AD.

Keywords: Alzheimer's disease, F-PACK, Polygenic risk score, Amyloid-PET, Longitudinal study

Background

Alzheimer's disease (AD) is the most common form of dementia in the global population, with a complex interplay of both genetic and environmental factors [1]. Changes observed in AD, such as the accumulation of brain amyloid-β protein, can occur more than a decade prior to symptom onset (the preclinical or asymptomatic phase) [2]. Age is one of the largest risk factors for AD risk, where many of the observed pathological changes occur as age increases [3]. It is of high importance to develop methods that detect those individuals at risk of developing the disease prior to symptom onset, as this phase presents a window of opportunity for early disease diagnosis, treatment administration, and determining individuals suitable for prevention trials.

Apolipoprotein E ε4 (*APOE4*) is the largest genetic risk factor for development of sporadic AD [4] and has been

†Isabelle Cleynen and Rik Vandenberghe contributed equally.

*Correspondence: rik.vandenberghe@uzleuven.be

[9] Neurology Department, University Hospitals Leuven, Herestraat 49, 3000 Leuven, Belgium
Full list of author information is available at the end of the article

shown to increase amyloid deposition in a dose-dependent manner, in the asymptomatic, the mild cognitive impairment and the dementia stages of AD [5–7]. Accumulation of brain amyloid in the asymptomatic phase occurs in a sigmoidal fashion, prior to reaching a plateau [8]. However, genetic risk for amyloid accumulation is largely unknown above the known effect of *APOE4*.

Beyond *APOE*, recent large-scale genome-wide association studies (GWAS) have highlighted low effect size variants in non-*APOE* genes that modify AD dementia risk [9–13]. In isolation, the identified risk SNPs have limited use in predicting AD risk. Combinations of selected AD risk SNP scores have previously been implemented in case-control studies, and have shown an increased risk of AD with a higher score (e.g. [14]). A polygenic risk score (PRS) approach to disease risk prediction is able to take into consideration all SNPs that show an association with AD, despite their small effect sizes, by capturing the overall genetic risk for an individual into a single score. This has already been performed in AD case-control studies (e.g. [14–16]), but there is a requirement for investigation in the asymptomatic phase, as well as determining the genetic risk for amyloid accumulation.

There are still many factors unknown about how to best model the PRS, for example the optimal threshold for SNP inclusion (pT) and how to represent the effect of *APOE* (e.g. for AD risk). A seminal study from Escott-Price et al. [15] suggested a PRS with the highest prediction accuracy (AUC = 78.2%) in predicting AD cases from controls is built using a liberal threshold for SNP inclusion ($pT < 0.5$), suggesting a polygenic architecture to AD. However, more recent studies have implied a more oligogenic architecture to AD, in which there are fewer SNPs associated with disease risk [17]. This suggests the use of more stringent (closer to genome-wide significant) pTs for the calculation of PRS for AD.

A more recent study from Leonenko et al. [18] further evaluated how best to model the *APOE4* effect in the context of PRS and found that the best prediction accuracy to predict AD cases from controls (AUC = 74.1%) came from a combination of a PRS excluding the *APOE* region with the addition of the weighted sum of two directly genotyped *APOE ε2* and *ε4* alleles (rs429358, rs7412, $PRS_{noAPOE}+APOE_{\varepsilon2+\varepsilon4}$) and a threshold $pT < 0.1$. This was when comparing PRS built using different SNP combinations, including PRS_{noAPOE} and PRS including all possible SNPs, at varying thresholds.

We aimed to evaluate PRS built as $PRS_{noAPOE}+APOE_{\varepsilon2+\varepsilon4}$, using different thresholds for SNP inclusion to determine the association with amyloid accumulation. We included cognitively intact older individuals participating in the Flemish Prevent AD Cohort KU Leuven (F-PACK), some of whom are in the asymptomatic stage of AD. We compared the performance of $PRS_{noAPOE}+APOE_{\varepsilon2+\varepsilon4}$ to other PRS.

Methods

Study participants

The Laboratory for Cognitive Neurology follows a cohort of 180 community-recruited deeply phenotyped older adults, known as F-PACK. F-PACK individuals were recruited between 2009 and 2015 in three waves of 60 individuals. At recruitment, individuals had to be aged between 50 and 80 years old, score ≥ 27 on the mini mental state examination (MMSE) and score zero on the clinical dementia rating (CDR) scale. Furthermore, individuals had to score within published norms on an extensive neuropsychological test battery [19, 20]. Exclusion criteria included a history of neurological or psychiatric illness, contraindication for magnetic resonance imaging (MRI), focal brain lesions on MRI, history of cancer, or exposure to radiation one year preceding the baseline amyloid positron emission tomography (PET) scan. Recruitment was stratified for two genetic factors: *APOE4* allele (present or absent) and *BDNF* status (*66 met* allele present or absent). This was carried out such that per 5-year age bin each factorial cell contained the same number of individuals matched for age, sex, and education. All recruited individuals received structural MRI and an ^{18}F-Flutemetamol amyloid-PET scan at baseline. Participants are invited for 2-yearly neuropsychological assessments over a 10-year period.

F-PACK individuals received blood collection for genotyping at recruitment. A subset of 90 participants have additionally received a follow-up amyloid-PET scan, on average 6.1 (3.4–10.9) years after baseline.

The protocol was approved by the Ethics Committee University Hospitals Leuven. All participants provided written informed consent in accordance with the declaration of Helsinki.

Structural MRI acquisition

At baseline and follow-up, each participant received a high resolution T1-weighted structural MRI scan for the PET processing procedure described below. Scans were performed using a 3T Philips Achieva dstream 32-channel headcoil MRI scanner (Philips, Best, The Netherlands). All baseline and 69 follow-up scans were acquired using the same 3D turbo field echo sequence: repetition time = 9.6 ms; echo time = 4.6 ms; flip angle = 8°; field of view = 250 × 250 mm; 182 slices; voxel size 0.98 × 0.98 × 1.2 mm^3. Eighteen follow-up scans were acquired using a three-dimensional magnetisation-prepared rapid

gradient-echo sequence, due to being acquired as part of The Amyloid Imaging to Prevent Alzheimer's Disease study (AMYPAD): repetition time = 6.6 ms; echo time = 3.1 ms; flip angle = 9°; field of view = 270 × 252 mm; 170 slices; voxel size 1.05 × 1.05 × 1.2 mm^3. Three individuals refused a follow-up scan.

^{18}F-Flutemetamol PET acquisition and pre-processing

As previously described, ^{18}F-Flutemetamol PET scans were acquired on a 16-slice Biograph PET/CT scanner (Siemens, Erlangen, Germany) at baseline and follow-up (6.1 (3.4–10.9) years), with a net injected intravenous dose of 149 MBq (127–162 MBq) and 156 MBq (77–198 MBq), respectively, with an acquisition window of 90–120 min post-injection [19, 21–24]. Four follow-up PET scans had an acquisition window of 90–110 min due to acquisition prior to a protocol amendment. A low-dose CT scan was acquired prior to all scans for attenuation correction. Random and scatter corrections were applied. Scans were reconstructed as frames of five minutes. All scans were reconstructed using ordered subsets expectation maximisation. All baseline scans and 73 follow-up scans were reconstructed as five iterations in eight subsets. Sixteen follow-up scans were reconstructed as four iterations in 21 subsets, due to being reconstructed as part of AMYPAD. The spatial resolution of the scanner is 4.6 mm full width at half maximum 1cm off centre measured with the NEMA protocol, and all scans were smoothed with a 5-mm full width at half maximum Gaussian filter.

^{18}F-Flutemetamol image analysis

Statistical Parametric Mapping version 12 (SPM12, Wellcome Trust Centre for Neuroimaging, London, UK, http://www.fil.ionucl.ac.uk/spm) running on MATLAB R2018b (Mathworks, Natick, MA, USA) was used to process the images, as described previously [19, 21–24].

We calculated (mean) standardised uptake value ratios (SUVRs) from the spatially normalised images (voxel size: 2 × 2 × 2 mm^3) in a composite cortical volume of interest ($SUVR_{comp}$) based on the automated anatomical labelling atlas (AAL). This composite volume of interest included the following bilateral regions: frontal (AAL areas 3–10, 13–16, 23–28), parietal (AAL 57–70), anterior cingulate (AAL 31–32), posterior cingulate (AAL 35–36), and lateral temporal (AAL 81–82, 85–90) and was masked with the participant-specific grey matter (GM) segmentation map (threshold = 0.3) [19, 25]. Cerebellar grey matter was used as the reference region to calculate $SUVR_{comp}$, defined as AAL areas 91–108 and was masked by the participant-specific GM map (intensity threshold = 0.3) [19]. $SUVR_{comp}$ were then converted to Centiloids (CL) using the formula $CL = 127.6 \times SUVR_{comp} - 149$ [26, 27]. Individuals were deemed amyloid positive when their CL was ≥ 23.5, a pathologically confirmed cut-off for amyloid positivity [28]. Furthermore, to model amyloid change longitudinally, we calculated rate of change as:

$$Amyloid\ rate\ of\ change = \frac{Follow-up\ Centiloid - Baseline\ Centiloid}{Time\ interval\ (years)}$$

For use in secondary analyses, we repeated the PET image processing pipeline including a partial volume correction (PVC, 5 mm full-width half-maximum) step, using a modified Müller-Gärtner procedure [29]. Rate of change was derived, as per the above equation using SUVRs, of these corrected images for use in the analyses described below.

Structural MRI longitudinal change

In a secondary analysis, we also examined whether any PRS with significant predictive value for amyloid accumulation also had any predictive value for longitudinal MRI volume loss. As a measure of atrophy, we used the GM maps at baseline and follow-up, produced from the PET processing procedure, to calculate the percental whole brain GM volume change between the two time points as:

$$\frac{Grey\ matter\ volume\ at\ baseline - Grey\ matter\ volume\ at\ follow-up}{Grey\ matter\ volume\ at\ baseline}\ x\ 100$$

Furthermore, for a voxelwise analysis we calculated GM change images, as follow-up GM map minus baseline GM map, using SPM12, for use in voxelwise regression analyses described below.

Modelling of longitudinal cognitive change

For the PRS with predictive value for amyloid accumulation, we also examined whether this predictive power extended to cognitive change. To model cognitive

change, based on a prior study [20], the mean Buschke Selective Reminding Test Total Retention (BSRT TR) score [30] was selected and slopes were calculated using latent growth curve analysis, using the R package *Lavaan* [31]. Individuals are being followed for a period of 10 years with two-yearly neuropsychological evaluations, so we used mean BSRT TR scores from all available neuropsychological testing time points (FUY) up until the closest to the follow-up amyloid-PET scan (number of individuals at each FUY: 4 FUY2, 37 FUY4, 32 FUY6, 10 FUY8, 7 FUY10; mean interval between follow-up amyloid-PET and closest neuropsychological assessment is 13.06 ± 12.04 months). Missing values were imputed in R using the CART imputation method in the package *mice* [32]. The calculated mean BSRT TR slopes were then used further, where a more negative slope represents steeper decline.

Genetic data acquisition and processing

DNA was further available for 177 F-PACK participants, which was subsequently genotyped using the Illumina Global Screening Array (GSA, coverage of 657,598 SNPS) in collaboration with the Institute of Clinical and Medical Biology (University Hospital Schleswig-Holstein, Germany) [33]. Standard quality control (QC) was performed using PLINK (Version 1.9, www.cog-genomics.org/plink/1.9) and included SNP call rate ≥ 0.95, minor allele frequency (MAF) ≥ 0.01, and outlying heterozygosity (± 5 standard deviations) [34]. Hardy-Weinberg equilibrium threshold $= 1 \times 10^{-6}$ was also applied. Ethnic outliers were detected using the Phase 3 1000 Genomes (1KG) dataset ($N = 2504$ [35]). Imputation was performed using the Michigan Imputation Server (https://imputationserver.sph.umich.edu) [36] and Haplotype Reference Consortium reference panel (http://www.haplotype-reference-consortium.org), resulting in 39,131,578 SNPs. Data were filtered with imputation information score > 0.7 and MAF ≥ 0.01. After imputation and QC 7,466,483 SNPs remained for further analysis. Three individuals were removed during the QC process (one due to sample duplication, one due to relatedness (pi-hat > 0.2), and one due to outlying heterozygosity).

Polygenic risk score calculation

PRS calculations were performed using PRSice-2 [37]. The stage 1 summary statistics from the GWAS performed by Kunkle et al. [11] were used as the base file, and the European individuals from 1KG ($N = 503$ [35]) were used as an external reference panel for clumping to remove SNPs in high linkage disequilibrium (clumping window = 250 kilobases, $r^2 = 0.1$). Post-clumping, there were 335,326 SNPs remaining for PRS calculations. We first calculated PRS using the $PRS_{noAPOE}+APOE_{\varepsilon 2+\varepsilon 4}$ approach [18]. We calculated PRS excluding the *APOE* region (chromosome 19: 45-48.8 Mb, PRS_{noAPOE}) at three thresholds for SNP inclusion (pT): pT = 0.1; 1×10^{-5}; 5×10^{-8}, and then added the weighted sum of the two major *APOE* SNPs (rs429358 and rs7412, $APOE_{\varepsilon 2+\varepsilon 4}$), using the effect sizes from Kunkle et al. [11], to each score (N1 * β1 + N2 * β2, where N1 and N2 are the number of alleles for each *APOE* SNP, respectively, and β1 and β2 are the corresponding effect sizes).

For comparison, we also calculated PRS_{AD}, in which all available SNPs were included at each pT, as well as $PRS_{APOEonly}$, in which PRS were calculated at each pT using only the *APOE* region specified above. All PRS were *z*-score normalised prior to further analyses.

Statistical analyses

Statistical analyses were performed in R version 4.1.0 (2021-05-18; The R Foundation for Statistical Computing; https://cran.r-project.org/). Prior to analyses, Shapiro-Wilk tests were used to determine data normality.

Cohort characteristics were assessed between *APOE4* carriers and non-carriers using Wilcoxon rank sum tests with continuity correction or Welch two-sample *t*-tests for continuous data, depending on normality, and χ^2 tests for categorical data.

Primary analyses

For our primary analysis, linear regressions were performed for each $PRS_{noAPOE}+APOE_{\varepsilon 2+\varepsilon 4}$ (i.e. at 3 different SNP inclusion thresholds) as predictor, and amyloid rate of change as outcome variable. Baseline age, sex, and the first three principal components were included as covariates. Inference was based on an uncorrected $p < 0.05$ threshold divided by the number of SNP inclusion thresholds ($N = 3$).

Secondary analyses

We investigated how $PRS_{noAPOE}+APOE_{\varepsilon 2+\varepsilon 4}$ performed compared to other PRS, thus linear regressions were also performed as described above with PRS_{AD}, $APOE_{\varepsilon 2+\varepsilon 4}$, PRS_{noAPOE}, or with $PRS_{APOEonly}$. Per type of PRS, inference was based on an uncorrected $p < 0.05$ threshold divided by the number of SNP inclusion thresholds ($N = 3$), except for $APOE_{\varepsilon 2+\varepsilon 4}$ given that this score does not rely on *p*-value thresholds for SNP inclusion as it is built using only the weighted sum of two *APOE* SNPs. We also investigated whether all calculated PRS were associated with baseline amyloid burden using the same statistical approach.

In a further secondary analysis, we determined the ability for any significant PRS to discriminate individuals who were amyloid negative at both time points, on the one hand, from individuals who were amyloid negative at baseline and positive at follow-up or amyloid positive at both time points, on the other hand. We performed a set of receiver operating characteristic (ROC) analyses using the R package *pROC* based on a logistic regression classifier [38]. We included two demographic models (one model with age + sex; one model with age + sex + *APOE4* status (yes/no)) and models including any significant PRS determined from the previous analyses, with age and sex. Measures of performance are given as areas under the curve (AUCs) and 95% confidence intervals (CI). Pairwise comparisons of model AUCs were performed using the DeLong method [39].

To evaluate the effect of PVC, we also carried out the regression analyses with the longitudinal change in PVC SUVRs as predictor.

Finally, we performed the regression analyses for cognitive decline or GM atrophy, with any PRS that had a significant association with amyloid rate of change. In addition, we performed whole-brain voxelwise *t*-tests using the GM change maps, with the significant PRS and time interval as covariates. We used a FWE corrected cluster-level threshold of $p < 0.05$ with the voxel-level set at uncorrected $p < 0.001$ [40].

Results

F-PACK characteristics

From the 90 F-PACK individuals with follow-up amyloid-PET included in this study, nine were amyloid positive at baseline (10%) and 21 at follow-up (23%, Table 1, Fig. 1). *APOE4* carriers had a significantly higher amyloid rate of change (rate of change for *APOE4* carriers: 1.06 (range: −2.85–13.92); *APOE4* non-carriers: −0.03 (range: −3.03–4.22) $p = 0.01$, outlier excluded $p = 0.02$) and a significantly lower time interval between amyloid-PET scans than non-carriers (time interval for *APOE4*

Table 1 Baseline F-PACK characteristics stratified for *APOE4* polymorphism status for individuals with baseline and follow-up amyloid-PET. Data are reported as median and range (minimum to maximum) for continuous variables and numerical for categorical variables. Wilcoxon rank sum test with continuity correction or Welch two-sample *t*-tests were used for continuous data, depending on data normality. χ^2 tests have been used for categorical data. *ε2ε3* $N = 7$; *ε2ε4* $N = 2$; *ε3ε3* $N = 42$; *ε3ε4* $N = 37$; *ε4ε4* $N = 2$. Total $N = 90$

	***APOE4* non-carrier (*n*=49)**	***APOE4* carrier (*n*=41)**	**Statistics**
Sex (male/female)	24/25	22/19	$X^2 = 0.05, p = 0.82$
BDNF *66 met* carriers	24	23	$X^2 = 0.21, p = 0.64$
Age (years)	67 (52–80)	68 (56–79)	$T = -0.18, p = 0.86$
Education (years)	14 (8–20)	16 (9–23.5)	$T = 1.76, p = 0.08$
MMSE	29 (27–30)	29 (27–30)	$W = 1022.5, p = 0.88$
CDR	0	0	*NA*
AVLT TL (/75)	47 (30–69)	46 (35–68)	$T = -0.16, p = 0.87$
AVLT %DR	85.7 (30–107.7)	86.7 (58.3–107.7)	$W = 1039.5, p = 0.78$
BSRT TR (/12)	8.2 (5.6–10.8)	7.9 (4.9–10.5)	$T = -0.94, p = 0.35$
BSRT DR (/12)	8 (2–12)	8 (3–12)	$W = 932.5, p = 0.56$
BNT (/60)	57 (46–60)	57 (41–60)	$W = 1028.5, p = 0.85$
AVF (# words)	23 (14–40)	23 (14–42)	$T = 0.50, p = 0.62$
LVF (# words)	36 (14–65)	37 (9–61)	$T = -0.05, p = 0.96$
PALPA49 (/30)	28 (20–30)	27 (23–30)	$W = 981.5, p = 0.85$
RPM (/60)	46 (22–57)	45 (22–57)	$W = 864, p = 0.26$
TMT B/A	2.2 (1.2–4.8)	2.4 (1.0–4.8)	$T = 0.69, p = 0.49$
Baseline Centiloid	4.8 (−14.1–99.8)	7.7 (−14.8–116.8)	$W = 1163, p = 0.20$
Baseline amyloid positivity	4 (8%)	5 (12%)	$X^2 = 0.08, p = 0.78$
Follow-up amyloid positivity	7 (14%)	14 (34%)	$X^2 = 3.87, p = 0.049$
Amyloid rate of change	−0.03 (−3.03–4.22)	1.06 (−2.85–13.92)	$W = 1313, p = 0.01$
Time interval (years)	6.1 (4.0–10.9)	5.4 (3.4–10.0)	$W = 675, p = 0.008$

Abbreviations: *AVF* Animal Verbal Fluency Test, *AVLT TL/DR* Rey Auditory Verbal Learning Test Total Learning/Delayed Recall, *BNT* Boston Naming Test, *BSRT TR/DR* Buschke Selective Reminding Test Total Retention/Delayed Recall, *CDR* Clinical Dementia Rating scale, *LVF* Letter Verbal Fluency Test, *MMSE* Mini Mental State Examination, *PALPA49* Psycholinguistic Assessment of Language Processing in Aphasia (PALPA) subtest 49, *RPM* Raven's Progressive Matrices, *TMT B/A* Trail Making Test part B divided by part A

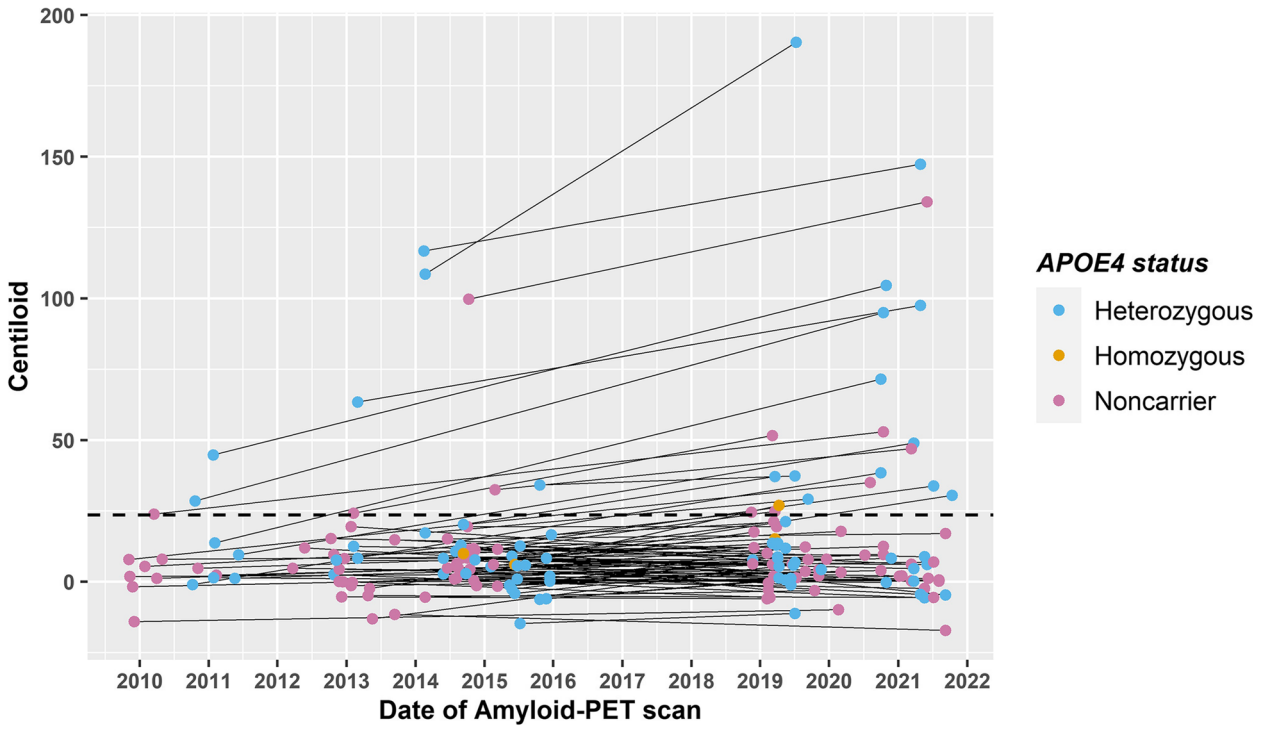

Fig. 1 Change in amyloid load between baseline and follow-up for F-PACK participants, expressed in Centiloids. The dotted line represents the threshold for amyloid positivity ≥ 23.5 [28]. $N = 90$

carriers: 5.4 (range: 3.4–10.0) years; *APOE4* non-carriers 6.1 (range: 4.0–10.9) years, $p = 0.008$). There was also a significantly higher number of *APOE4* carriers classified as amyloid positive at follow-up (34%) compared to non-carriers (14%, $p = 0.049$). Two individuals had a CDR that had evolved to 0.5 at the time of follow-up amyloid-PET.

There was an outlier with amyloid rate of change (as determined by Grubb's test in R, using the package *Outliers*). Therefore, the amyloid analyses were repeated excluding this individual.

Primary analyses: PRS_{noAPOE}+$APOE_{\varepsilon 2+\varepsilon 4}$

PRS_{noAPOE}+$APOE_{\varepsilon 2+\varepsilon 4}$ had a significant association with amyloid rate of change when the SNP inclusion threshold (pT) $= 5 \times 10^{-8}$ ($p = 0.0126$, $\beta = 0.68$ (95% CI 0.15, 1.20), $R^2 = 0.12$, Figs. 2 and 3A, Table 2). When the outlier was removed, significance remained ($p = 0.004$, $\beta = 0.65$ (95% CI 0.21, 1.09), $R^2 = 0.11$, Fig. 3B). Figure 2 shows that the highest R^2 and lowest p-value occur when the pT is more stringent.

Both regression plots in Fig. 3A and B highlight increasing amyloid rate of change with increasing PRS. One can also appreciate the lower PRS are for those participants with $\varepsilon 2\varepsilon 3$ or $\varepsilon 3\varepsilon 3$ *APOE* genotypes, whereas, in general, those participants with higher PRS carry at least one $\varepsilon 4$ allele. No significance was found at the other pTs.

Secondary analyses: other PRS models and phenotypes

From our secondary analyses, there was a significant association between amyloid rate of change and $APOE_{\varepsilon 2+\varepsilon 4}$ ($p = 0.0496$, $\beta = 0.56$ (95% CI 0.0009, 1.09), $R^2 = 0.09$, Fig. 2, Table 2). When the outlier was removed, the significance remained ($p = 0.0201$, $\beta = 0.56$ (95% CI 0.09-1.00), $R^2 = 0.08$). None of the other PRS were significant with the total group. The results from the total cohort can be observed in Fig. 2, where red points represent significant p-values, and blue points are non-significant. From the figure, one can also appreciate the higher variance explained by the PRS on amyloid accumulation in the regressions when using the more stringent SNP inclusion thresholds. Of note is the higher R^2 with PRS_{noAPOE}+$APOE_{\varepsilon 2+\varepsilon 4}$ when pT $= 5 \times 10^{-8}$ ($R^2 = 0.12$) compared to when using $APOE_{\varepsilon 2+\varepsilon 4}$ alone ($R^2 = 0.09$). No PRS were associated with baseline amyloid load (Supplementary Table 1).

After performing PVC, the p-value for PRS_{noAPOE}+$APOE_{\varepsilon 2+\varepsilon 4}$ at pT $= 5 \times 10^{-8}$ was comparable to that obtained without PVC (values for PVC SUVRs: $p = 0.0196$ ($\beta = 0.008$ (95% CI 0.001, 0.014), $R^2 = 0.13$). Note that we used SUVRs for the PVC analysis; hence, this has to be compared with the same analysis for the primary analysis using SUVRs as well. At pT $= 5 \times 10^{-8}$, the regression output for the primary analysis with

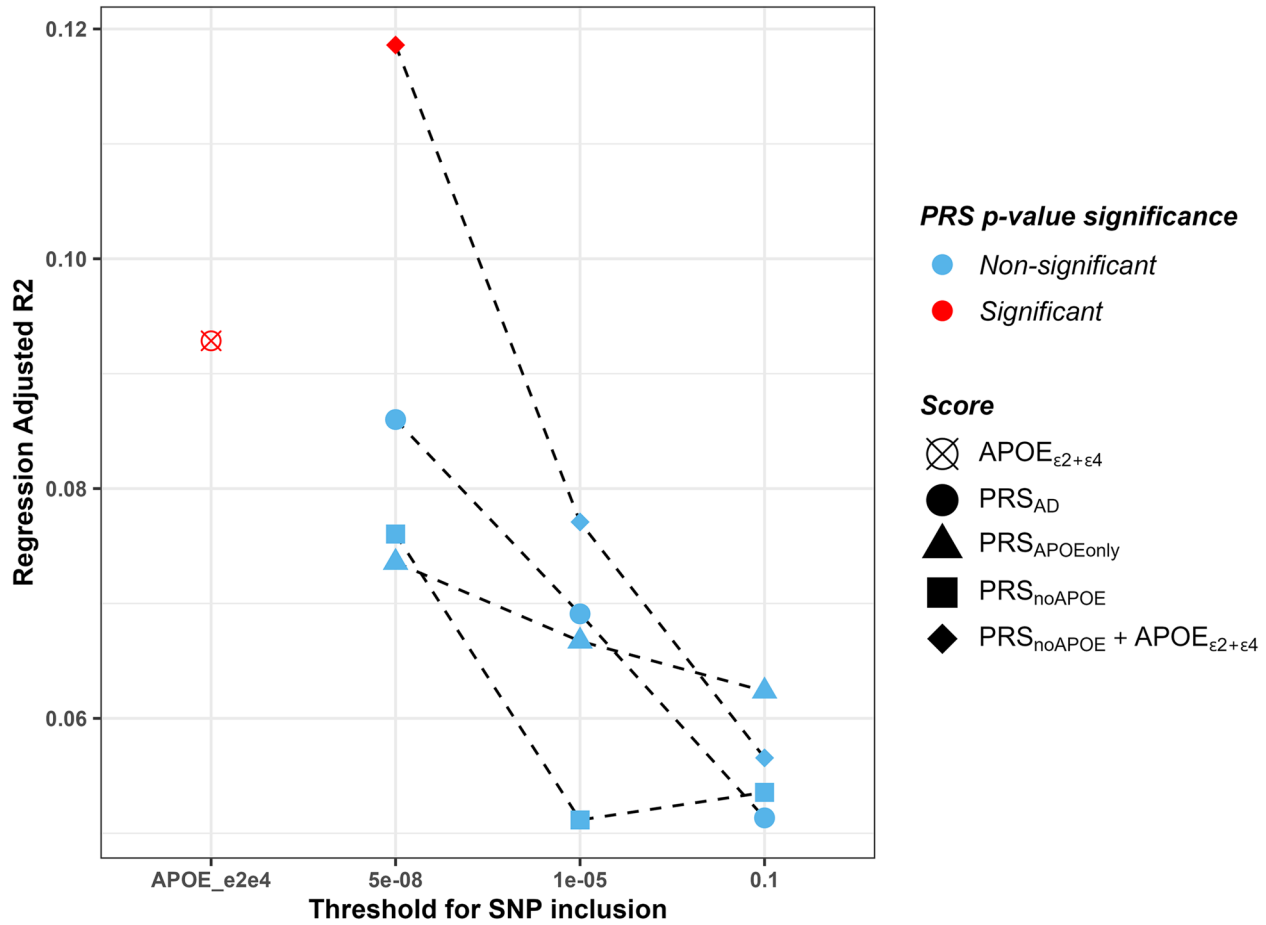

Fig. 2 The adjusted R^2 and PRS *p*-values for the regression models. The red points represent significant PRS *p*-values from the regression models (< 0.017 (multiple pT), or < 0.05 (for single score)). The higher the adjusted R^2 the higher the variance explained by the PRS on amyloid rate of change in the linear regression model. $N = 90$

non-PVC SUVRs is $p = 0.0131$ ($\beta = 0.005$ (95% CI 0.001, 0.009), $R^2 = 0.11$). Significance was lost for $APOE_{\varepsilon 2+\varepsilon 4}$ ($p = 0.30$, $\beta = 0.005$ (95% CI −0.002, 0.011), $R^2 = 0.10$) after PVC correction. For comparison, the regression output with SUVRs for $APOE_{\varepsilon 2+\varepsilon 4}$ correspond to: $p = 0.051$, $\beta = 0.004$ (95% CI −0.00002, 0.009), $R^2 = 0.08$).

Figure 4 shows the results from the ROC analysis. We determined the ability of PRS_{noAPOE}+$APOE_{\varepsilon 2+\varepsilon 4}$ and of $APOE_{\varepsilon 2+\varepsilon 4}$ to discriminate amyloid negative individuals at both time points, on the one hand, from individuals who were amyloid negative at baseline and positive at follow-up or amyloid positive at both time points, on the other hand. The best performing model was age + sex + PRS_{noAPOE}+$APOE_{\varepsilon 2+\varepsilon 4}$ with pT $= 5 \times 10^{-8}$ (AUC = 0.74, 95% CI = 0.62–0.86). Numerically, the second best performing model was the demographic model consisting of age + sex + *APOE4* status (yes/no) (AUC = 0.71, 95% CI = 0.58–0.84). This had a similar performance to the model with age + sex + $APOE_{\varepsilon 2+\varepsilon 4}$ (AUC = 0.70, 95% CI = 0.57–0.83). The demographic model including age + sex (AUC = 0.63, 95% CI = 0.51–0.75) performed the worst. None of the models were significantly different from each other when performing pairwise model comparisons (Supplementary Table 2).

PRS_{noAPOE}+$APOE_{\varepsilon 2+\varepsilon 4}$ and $APOE_{\varepsilon 2+\varepsilon 4}$ were not associated with cognitive decline over the time course measured. Neither were these PRS associated with longitudinal whole-brain grey matter atrophy nor were there significant effects based on the whole-brain voxelwise analyses (Supplementary Table 3).

Discussion

Our study has highlighted that specific AD PRS are associated with amyloid accumulation in the asymptomatic phase of the disease, when built using a stringent SNP inclusion threshold.

The present study primarily investigated the association of amyloid change and PRS_{noAPOE}+$APOE_{\varepsilon 2+\varepsilon 4}$, given

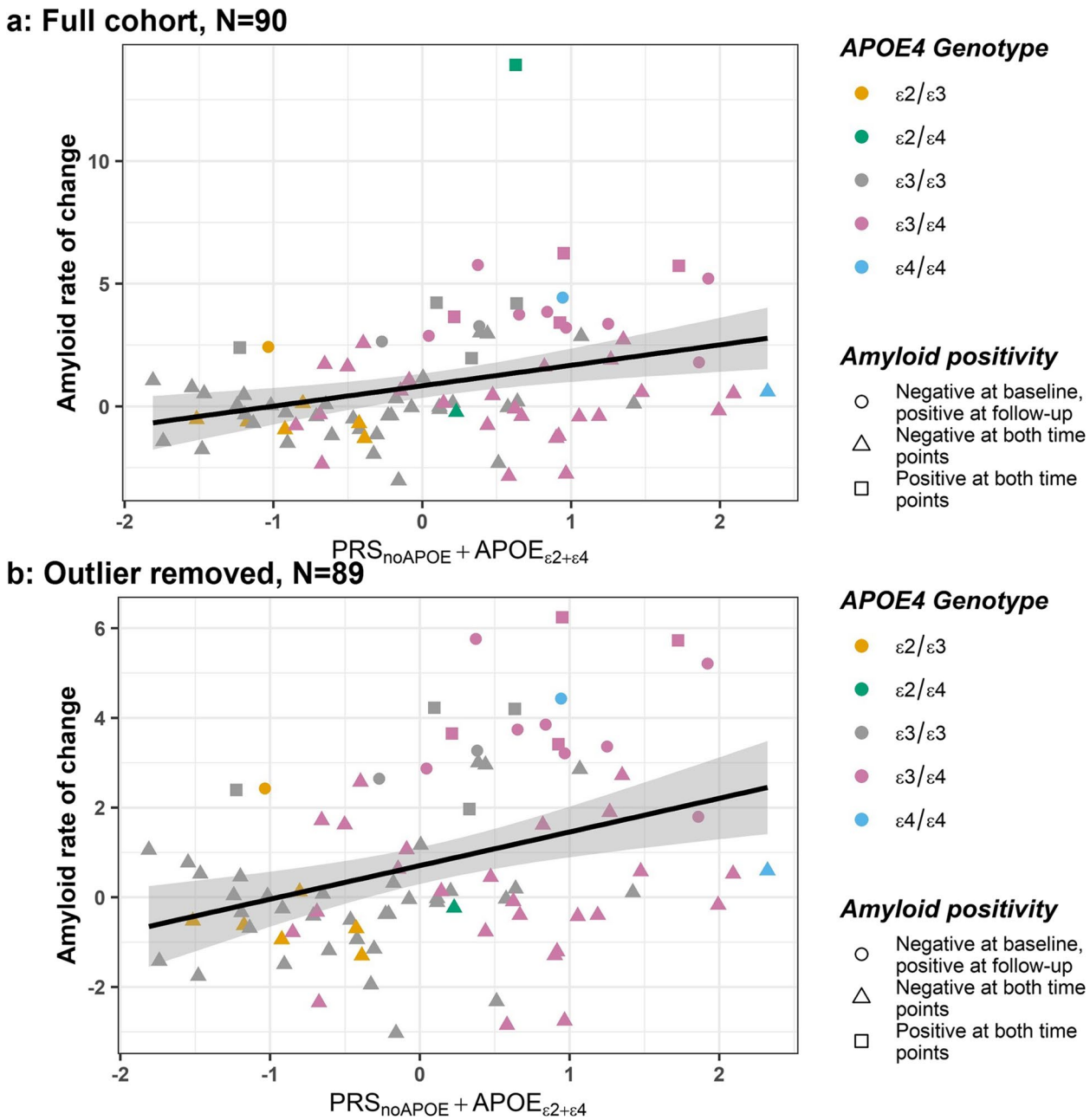

Fig. 3 Regression plots for PRS$_{noAPOE}$+*APOE*$_{ε2+ε4}$ at pT = 5×10^{-8} and amyloid rate of change. **A** For the whole cohort. *N* = 90. **B** When the outlier for amyloid rate of change is removed. *N* = 89. The shape indicates amyloid status based on CL ≥ 23.5 [27]: amyloid negative at both time points (triangle, *N* = 69); amyloid negative at baseline and amyloid positive at follow-up (circle, *N* = 12); and amyloid positive at both time points (square, *N* = 9). Amyloid rate of change is follow-up Centiloid minus baseline Centiloid, divided by the time interval (years). Participants are coloured based on *APOE4* genotype (*ε2ε3 N* = 7; *ε2ε4 N* = 2; *ε3ε3 N* = 42; *ε3ε4 N* = 37; *ε4ε4 N* = 2; outlier is *ε2ε4*)

PRS built in this way have recently been shown to give the best prediction accuracy to predict AD cases from controls (AUC = 74.1%) with pT < 0.1 [18]. In this previous paper, this PRS was superior at predicting AD cases from controls, compared to PRS built using different SNP combinations, including PRS$_{noAPOE}$ and PRS$_{AD}$, at varying thresholds. In that study, the best prediction accuracy for PRS$_{AD}$ reached an AUC of 69.8% (pT = 5×10^{-8}) and PRS$_{noAPOE}$ AUC = 61.3% (pT = 0.1). Furthermore, these were not better performing than the two major *APOE*

Table 2 Regression results for the different PRS and amyloid rate of change. Raw values are shown, significant *p*-values in bold (< 0.017 (multiple pT) or < 0.05 (for single score)). *APOE* region: chromosome 19: 45–48.8 Mb. *APOE* SNPs: rs429358, rs7412. Baseline age, sex, and PCs 1–3 included as covariates. $N = 90$

Score	Score description	pT	Number of SNPs	Adjusted R^2	PRS *p*-value	PRS β (95% CI)
PRS_{noAPOE}+$APOE_{\varepsilon2+\varepsilon4}$	All available SNPs at each pT excluding the *APOE* region, plus the weighted sum of the two major *APOE* SNPs	5×10^{-8}	22	0.12	**0.0126**	0.68 (0.15–1.20)
		1×10^{-5}	70	0.08	0.1188	0.45 (−0.12–1.02)
		0.1	77,270	0.06	0.4319	0.21 (−0.32–0.74)
PRS_{AD}	All available SNPs at each pT	5×10^{-8}	65	0.09	0.0721	0.48 (−0.04–1.01)
		1×10^{-5}	129	0.07	0.1895	0.36 (−0.18–0.89)
		0.1	77,378	0.05	0.6874	−0.10 (−0.61–0.40)
$APOE_{\varepsilon2+\varepsilon4}$	Weighted sum of the two major *APOE* SNPs		2	0.09	**0.0496**	0.55 (0.0009–1.09)
PRS_{noAPOE}	All available SNPs at each pT excluding the *APOE* region	5×10^{-8}	20	0.08	0.1262	0.37 (−0.10–0.84)
		1×10^{-5}	68	0.05	0.7016	0.10 (−0.43–0.64)
		0.1	77,268	0.05	0.5510	−0.15 (−0.66–0.35)
$PRS_{APOEonly}$	All available SNPs within the *APOE* region at each pT	5×10^{-8}	46	0.07	0.1455	0.39 (−0.14–0.91)
		1×10^{-5}	62	0.07	0.2191	0.33 (−0.20–0.86)
		0.1	118	0.06	0.2885	0.29 (−0.25–0.82)

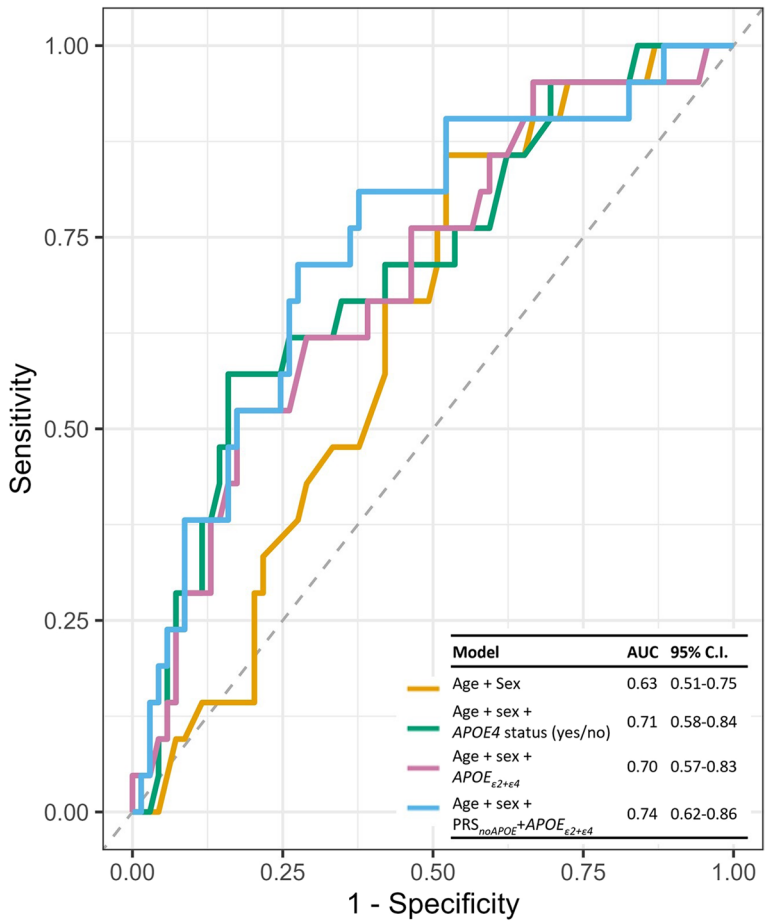

Fig. 4 ROC curves for predicting amyloid status. PRS_{noAPOE}+$APOE_{\varepsilon2+\varepsilon4}$ (with $pT = 5 \times 10^{-8}$) with age and sex was numerically the best performing model at predicting individuals who were amyloid negative at both time points, on the one hand, from individuals who were amyloid negative at baseline and positive at follow-up or amyloid positive at both time points, on the other hand. Abbreviations: AUC, area under the curve; CI, confidence interval; ROC, receiver operating characteristic

SNPs (rs429358 and rs7412) alone (AUC = 70.0%) [18]. The data presented in the present study also suggest that PRS_{noAPOE}+$APOE_{\varepsilon 2+\varepsilon 4}$ with $pT = 5 \times 10^{-8}$ is superior than the other PRS at having an association with amyloid accumulation in the asymptomatic phase of AD. The effect sizes observed for this score are higher than those observed in the other models. This score had a more significant association with amyloid accumulation than the major *APOE* SNPs, in the linear regressions, and produced, numerically, the highest AUC (AUC = 74%) compared to the demographic models (AUC for age + sex = 63% and AUC for age + sex + *APOE4* status (yes/no) = 71%) and the model including the weighted sum of the two major *APOE* SNPs (AUC = 70%). The AUC of 74% is comparable to those reported in the literature in AD case-control prediction studies. This score also had a borderline significant association with amyloid rate of change after PVC was performed. The slight loss in significance is likely due to the introduction of additional noise from the PVC. This can occur when PVC is performed on PET scans of cognitively intact older adults, which pertains to the F-PACK cohort [41]. However, the results further strengthen the hypothesis that there are other variants above *APOE* that are important for amyloidogenic processes. The increasing levels of amyloid in this asymptomatic phase may be associated with these lower effect size variants, whereas in the latter disease stages these associations are absent due to amyloid accumulation reaching a plateau [8].

This study investigated whether the thresholds for SNP inclusion that were found to be optimal in AD case-control studies were also applicable in the asymptomatic phase to detect amyloid changes. The results show stringent thresholds for SNP inclusion have a significant association with amyloid accumulation compared to the more liberal threshold of pT = 0.1. More liberal thresholds may be optimal for predicting cases from controls, but the present study suggests when trying to detect amyloid accumulation in asymptomatic AD, stringent thresholds for SNP inclusion, that reduce noise, are more optimal.

Previous studies have been unable to demonstrate an association between PRS and amyloid accumulation (e.g. [42, 43]). It is consistently found in many studies that *APOE4* is associated with higher amyloid load and amyloid accumulation (in the asymptomatic phase [6, 44]), but the PRS-based studies were unable to provide evidence for an association between PRS and baseline amyloid nor PRS and amyloid accumulation. Consistent with previous studies, the data from the present study replicate the effect of *APOE4* on amyloid accumulation, as well as providing a lack of association between PRS and baseline amyloid load. However, the present study did find an association between a specific PRS and amyloid accumulation over time. It can be observed that some individuals in the F-PACK cohort exhibit negative rates of change, along with the individuals that increase. Figure 1 shows the change in amyloid over time for the F-PACK cohort. The range in amyloid load below the threshold is narrow, whereas the change in amyloid above threshold is much larger, highlighting that the most change is driven by changes above the threshold of amyloid positivity. This change is not occurring below the threshold and change is thus minimal, even with those participants with a negative amyloid rate of change. Furthermore, a sensitivity analysis was conducted, whereby we removed the individuals in whom amyloid increased but did not surpass the threshold for positivity, and the regression still produced significant results with $pT = 5 \times 10^{-8}$ (data not shown due to the introduction of potential bias from removing data a posteriori). However, this further strengthens the primary analysis results that the observed effect is not driven by spurious accumulations in amyloid. Thus, the use of PRS to predict amyloid accumulation in the asymptomatic phase allows for testing genetic determinants of the amyloidogenic processes in sporadic AD, in the absence of downstream secondary effects in this early disease stage.

The effect of the *APOE* variants is clearly high given the results presented. This highlights that in the asymptomatic stage *APOE4* has a large influence on the association of a PRS with amyloid change. When the threshold for SNP inclusion is more than genome-wide significant ($> 5 \times 10^{-8}$), the variance explained decreases, which is coupled with a loss in significance of the PRS. Thus, lower effect size variants play a role in AD risk, but increasing the threshold for SNP inclusion beyond genome-wide significance results in the addition of SNPs that create noise, thus suggesting an oligogenic architecture to (asymptomatic) AD. Nevertheless, the variance explained by the PRS on amyloid accumulation is low, thus there may be a large influence from other factors, such as gene-environment interactions.

Limitations

Some limitations need to be considered. The amyloid scans were acquired between 90 and 120 min post injection, and modelling of cerebral blood flow (CBF) changes over time was therefore not possible. According to a cross-sectional study in the Baltimore Longitudinal Study of Aging, amyloid SUVR can be influenced by CBF and mostly so in individuals with amyloid PET values in the upper tertile [45]. The effect of CBF on amyloid PET SUVR has been further quantified in a simulation study [46]. The increases in CBF that are needed to account for a 1% change in SUVR is of the order of 5–15% increase in CBF, and higher CBF changes are needed to affect

SUVR when amyloid load is lower ([46], Fig. 3). In a cognitively normal longitudinal cohort of individuals who remain relatively stable on a cognitive level and who do not manifest a neurological disease, a longitudinal CBF change of that order is implausible, also given the strict regulation of CBF under physiological circumstances. Note that CBF would need to increase over time with higher PRS scores. This can only be empirically excluded by concomitant longitudinal blood flow studies. The time interval between the baseline and follow-up amyloid-PET scans was variable, some individuals with a shorter interval than others. Amyloid accumulation is not a linear process; therefore, a difference in the onset of the rising phase of amyloid accumulation as well as the slope may be driving the differences we observe. The PRS were built using GWAS data from Kunkle et al. [11] that are not necessarily transferable to other ethnicities; thus, results should be carefully considered when inferring associations.

Conclusions

To conclude, a PRS built as $PRS_{noAPOE}+APOE_{\varepsilon 2+\varepsilon 4}$ with a stringent threshold for SNP inclusion had a more significant association with amyloid accumulation than the major *APOE* variants alone or than PRS built with other SNP combinations. This suggests an oligogenic, rather than polygenic, architecture to (asymptomatic) AD, in line with recent publications. The results may aid in participant recruitment and stratification for clinical trials, by identifying those individuals who are more susceptible to early brain amyloid changes, and thus more at risk to developing AD. According to the current dataset, $PRS_{noAPOE}+APOE_{\varepsilon 2+\varepsilon 4}$ outperforms the simple use of the *APOE4* polymorphism alone for this purpose.

Abbreviations

AAL: Automated anatomical labelling atlas; AD: Alzheimer's disease; APOE4: Apolipoprotein E ε4; AUC: Area under the curve; AVF: Animal Verbal Fluency; AVLT: Rey's Auditory Verbal Learning Test; BDNF: Brain-derived neurotrophic factor; BNT: Boston Naming Test; BSRT TR: Buschke Selective Reminding Test Total Retention; CBF: Cerebral blood flow; CI: Confidence interval; CDR: Clinical Dementia Rating; CGM: Cerebellar grey matter; CL: Centiloid; F-PACK: Flemish Prevent AD Cohort KU Leuven; FUY: Follow-up year neuropsychological testing time point; GM: Grey matter; GSA: Global Screening Array; GWAS: Genome-Wide Association Study; LVF: Letter Verbal Fluency; MAF: Minor allele frequency; MMSE: Mini Mental State Examination; MRI: Magnetic resonance imaging; PALPA49: Psycholinguistic Assessment of Language Processing in Aphasia item 49; PC: Principal component; PET: Positron emission tomography; PRS: Polygenic risk score; pT: *p*-value threshold for single nucleotide polymorphism inclusion; PVC: Partial volume correction; QC: Quality control; ROC: Receiver operating characteristic; RPM: Raven's Progressive Matrices; SNP: Single nucleotide polymorphism; SUVR: Standardised uptake value ratio; $SUVR_{comp}$: Standardised uptake value ratio in the composite cortical volume of interest; TMT: Trial Making Test; 1KG: 1000 Genomes.

Supplementary Information

The online version contains supplementary material available at https://doi.org/10.1186/s13195-022-01079-4.

Additional file 1: Supplementary Table 1. Regression results for PRS with baseline amyloid load. *APOE* SNPs: rs429358, rs7412. Baseline age, sex and PCs 1-3 included as covariates. $N = 90$. **Supplementary Table 2.** Model comparisons between Receiver Operating Characteristic Areas Under the Curve using the DeLong method. **Supplementary Table 3.** Regression results for the significant PRS with cognitive decline or grey matter atrophy. Raw values are shown. *APOE* SNPs: rs429358, rs7412. Baseline age, sex and PCs 1-3 included as covariates. $N = 90$.

Acknowledgements

We would like to thank Carine Schildermans and the staff of Nuclear Medicine and Neurology at the University Hospitals Leuven, in particular Kwinten Porters and Jef Van Loock, Karen Meersmans, Valerie Goovaerts, Astrid Hofkens, and Eva Dries.

Authors' contributions

RV and IC contributed to the study concept and design. KVL and PD aided with scheduling and processing PET data. KA and JS acquired baseline data. SV processed baseline blood samples for genotyping. ESL acquired follow-up neuroimaging data and performed all neuroimaging analyses. SDM generated the Centiloid conversion formula. ESL and YA generated the PRS. MR generated the mean Buschke slopes. ESL performed all statistical analyses, interpreted the data, made the figures, and drafted the manuscript. All authors contributed to critical revision and approval of the final manuscript.

Funding

This work was supported by the Foundation for Alzheimer Research SAO-FRMA (09013, 11020, 13007); Research Foundation Flanders (G094418N, G0F8516N and JPND-EraNet Triage G0G1519N); KU Leuven (C14/17/108 and C14/21/109); and Vlaams Agentschap voor Innovatie en Onderzoek HBC.2019.2523; ^{18}F-Flutemetamol for the baseline scans was provided by GE Healthcare free of charge for this academic investigator-driven trials.
The project leading to this application has received funding for the Innovative Medicines Initiative 2 Joint Undertaking under grant agreement No 115952 (http://www.imi.europa.eu). This joint undertaking receives the support from the European Union's Horizon 2020 research and innovation programme and EFPIA. This communication reflects the views of the authors and neither IMI nor the European Union and EFPIA are liable for any use that may be made of the information contained herein.
JS (12Y1620N) is a junior postdoctoral fellow and SDM is a doctoral fellow (11M0522N) of the Flanders Research Foundation (FWO, Fonds voor Wetenschappelijk Onderzoek, Belgium).

Availability of data and materials

Data are available upon reasonable request.

Declarations

Ethics approval and consent to participate

The protocol was approved by the Ethics Committee University Hospitals Leuven. All participants provided written informed consent in accordance with the declaration of Helsinki.

Consent for publication

Not applicable.

Competing interests

RV has received research grants from Research Foundation—Flanders (FWO) and KU Leuven, has had a clinical trial agreement for phase 1 and 2 study between University Hospitals Leuven and GE-HC, has received a non-financial support from GE-HC (provision of ^{18}F-Flutemetamol for conduct of investigator-driven trial free of cost), and has a clinical trial agreement (local principal investigator) between University Hospitals Leuven and Biogen, J&J, NovoNordisk, Roche, and UCB.

KVL has received research grants from FWO and KU Leuven, has clinical trial agreements through University Hospitals Leuven/KU Leuven and J&J, Merck, BMS, GE Healthcare, CHDI, Cerveau, Eikonizo, Lundbeck, UCB and Curasen. ESL, YA, MR, KA, JS, SV, SDM, PD, and IC have no disclosers.

Author details
[1]Laboratory for Cognitive Neurology, KU Leuven, Leuven, Belgium. [2]Alzheimer Research Centre KU Leuven, Leuven Brain Institute, Leuven, Belgium. [3]Laboratory for Complex Genetics, KU Leuven, Leuven, Belgium. [4]Bioclinica, Newark, CA, USA. [5]Translational Research Center for GastroIntestinal Disorders, Department of Chronic Diseases, Metabolism and Ageing, KU Leuven, Leuven, Belgium. [6]Laboratory of Molecular Neurobiomarker Research, KU Leuven, Leuven, Belgium. [7]Division of Nuclear Medicine, UZ Leuven, Leuven, Belgium. [8]Nuclear Medicine and Molecular Imaging, Department of Imaging and Pathology, KU Leuven, Leuven, Belgium. [9]Neurology Department, University Hospitals Leuven, Herestraat 49, 3000 Leuven, Belgium.

Received: 25 January 2022 Accepted: 8 September 2022
Published online: 23 September 2022

References

1. Gatz M, Reynolds CA, Fratiglioni L, Johansson B, Mortimer JA, Berg S, et al. Role of genes and environments for explaining Alzheimer disease. Arch Gen Psychiatry. 2006;63:168–74 American Medical Association.
2. Villemagne VL, Burnham S, Bourgeat P, Brown B, Ellis KA, Salvado O, et al. Amyloid β deposition, neurodegeneration, and cognitive decline in sporadic Alzheimer's disease: A prospective cohort study. Lancet Neurol. 2013;12:357–67.
3. Jack CR Jr, Knopman DS, Jagust WJ, et al. Hypothetical model of dynamic biomarkers of the Alzheimer's pathological cascade. Lancet Neurol. 2010;9(1):119–28. https://doi.org/10.1016/S1474-4422(09)70299-6.
4. Corder EH, Saunders AM, Strittmatter WJ, Schmechel DE, Gaskell PC, Small GW, et al. Gene dose of apolipoprotein E type 4 allele and the risk of Alzheimer's disease in late onset families. Science (1979). 1993;261:921–3 American Association for the Advancement of Science.
5. Grimmer T, Tholen S, Yousefi BH, Alexopoulos P, Förschler A, Förstl H, et al. Progression of cerebral amyloid load is associated with the apolipoprotein e ε4 genotype in Alzheimer's disease. Biol Psychiatry. 2010;68:879–84 NIH Public Access.
6. Villemagne VL, Pike KE, Chételat G, Ellis KA, Mulligan RS, Bourgeat P, et al. Longitudinal assessment of Aβ and cognition in aging and Alzheimer disease. Ann Neurol. 2011;69:181–92 NIH Public Access.
7. Yamazaki Y, Zhao N, Caulfield TR, Liu CC, Bu G. Apolipoprotein E and Alzheimer disease: pathobiology and targeting strategies. Nat Rev Neurol. 2019;15(9):501–18. https://doi.org/10.1038/s41582-019-0228-7.
8. Jack CR, Wiste HJ, Lesnick TG, Weigand SD, Knopman DS, Vemuri P, et al. Brain β-amyloid load approaches a plateau. Neurology. 2013;80:890–6 American Academy of Neurology.
9. Lambert JC, Ibrahim-Verbaas CA, Harold D, Naj AC, Sims R, Bellenguez C, et al. Meta-analysis of 74,046 individuals identifies 11 new susceptibility loci for Alzheimer's disease. Nat Genet. 2013;45:1452 NIH Public Access.
10. Jansen IE, Savage JE, Watanabe K, Bryois J, Williams DM, Steinberg S, et al. Genome-wide meta-analysis identifies new loci and functional pathways influencing Alzheimer's disease risk. Nat Genet. 2019;51:404–13 Nature Publishing Group.
11. Kunkle BW, Grenier-Boley B, Sims R, Bis JC, Damotte V, Naj AC, et al. Genetic meta-analysis of diagnosed Alzheimer's disease identifies new risk loci and implicates Aβ, tau, immunity and lipid processing. Nat Genet. 2019;51(3):414–30 [cited 2021 Dec 20], Nature Publishing Group; Available from: https://www.nature.com/articles/s41588-019-0358-2.
12. Wightman DP, Jansen IE, Savage JE, Shadrin AA, Bahrami S, Holland D, et al. A genome-wide association study with 1,126,563 individuals identifies new risk loci for Alzheimer's disease. Nat Genet. 2021;53:1276–82.
13. Bellenguez C, Küçükali F, Jansen IE, Kleineidam L, Moreno-Grau S, Amin N, et al. New insights into the genetic etiology of Alzheimer's disease and related dementias. Nat Genet. 2022;54:1–25 Nature Publishing Group; [cited 2022 Apr 13]. Available from: https://www.nature.com/articles/s41588-022-01024-z.
14. Sleegers K, Bettens K, De Roeck A, Van Cauwenberghe C, Cuyvers E, Verheijen J, et al. A 22-single nucleotide polymorphism Alzheimer's disease risk score correlates with family history, onset age, and cerebrospinal fluid Aβ42. Alzheimer's Dement. 2015;11:1452–60 Elsevier Inc.
15. Escott-Price V, Sims R, Bannister C, Harold D, Vronskaya M, Majounie E, et al. Common polygenic variation enhances risk prediction for Alzheimer's disease. Brain. 2015;138:3673–84 [cited 2019 Nov 29]. Available from: https://academic.oup.com/brain/article-lookup/doi/10.1093/brain/awv268.
16. Escott-Price V, Myers A, Huentelman M, Shoai M, Hardy J. Polygenic risk score analysis of Alzheimer's disease in cases without APOE4 or APOE2 alleles. J Prev Alzheimers Dis NLM (Medline). 2019;6:16–9.
17. Zhang Q, Sidorenko J, Couvy-Duchesne B, Marioni RE, Wright MJ, Goate AM, et al. Risk prediction of late-onset Alzheimer's disease implies an oligogenic architecture. Nat Commun. 2020;11:1–11 Nature Research.
18. Leonenko G, Baker E, Stevenson-Hoare J, Sierksma A, Fiers M, Williams J, et al. Identifying individuals with high risk of Alzheimer's disease using polygenic risk scores. Nat Commun. 2021;12:1–10 Nature Publishing Group; [cited 2021 Aug 5]. Available from: https://www.nature.com/articles/s41467-021-24082-z.
19. Adamczuk K, De Weer AS, Nelissen N, Chen K, Sleegers K, Bettens K, et al. Polymorphism of brain derived neurotrophic factor influences β amyloid load in cognitively intact apolipoprotein ε4 carriers. NeuroImage: Clin. 2013;2:512–20 Elsevier.
20. Schaeverbeke JM, Gabel S, Meersmans K, et al. Baseline cognition is the best predictor of 4-year cognitive change in cognitively intact older adults. Alz Res Therapy. 2021;13:75. https://doi.org/10.1186/s13195-021-00798-4.
21. Koole M, Lewis DM, Buckley C, Nelissen N, Vandenbulcke M, Brooks DJ, et al. Whole-body biodistribution and radiation dosimetry of 18F-GE067: a radioligand for in vivo brain amyloid imaging. J Nucl Med. 2009;50:818–22 Society of Nuclear Medicine.
22. Vandenberghe R, Van Laere K, Ivanoiu A, Salmon E, Bastin C, Triau E, et al. 18F-flutemetamol amyloid imaging in Alzheimer disease and mild cognitive impairment a phase 2 trial. Ann Neurol. 2010;68:319–29.
23. Vandenberghe R, Nelissen N, Salmon E, Ivanoiu A, Hasselbalch S, Andersen A, et al. Binary classification of 18F-flutemetamol PET using machine learning: Comparison with visual reads and structural MRI. Neuroimage. 2013;64:517–25.
24. Adamczuk K, Schaeverbeke J, Nelissen N, Neyens V, Vandenbulcke M, Goffin K, et al. Amyloid imaging in cognitively normal older adults: comparison between 18F-flutemetamol and 11C-Pittsburgh compound B. Eur J Nucl Med Mol Imaging. 2016;43:142–51 springer berlin.
25. Tzourio-Mazoyer N, Landeau B, Papathanassiou D, Crivello F, Etard O, Delcroix N, et al. Automated anatomical labeling of activations in SPM using a macroscopic anatomical parcellation of the MNI MRI single-subject brain. Neuroimage. 2002;15:273–89.
26. Klunk WE, Koeppe RA, Price JC, Benzinger TL, Devous MD, Jagust WJ, et al. The Centiloid project: standardizing quantitative amyloid plaque estimation by PET. Alzheimer's Dement. 2015;11:1–15.e4 Wiley.
27. De Meyer S, Schaeverbeke JM, Verberk IMW, Gille B, De Schaepdryver M, Luckett ES, et al. Comparison of ELISA- and SIMOA-based quantification of plasma Aβ ratios for early detection of cerebral amyloidosis. Alzheimer's Res Ther. 2020;12:162 BioMed Central Ltd.
28. la Joie R, Ayakta N, Seeley WW, Borys E, Boxer AL, DeCarli C, et al. Multisite study of the relationships between antemortem [11 C] PIB-PET Centiloid values and postmortem measures of Alzheimer's disease neuropathology. Alzheimer's Dement. 2019;15:205–16 NIH Public Access; [cited 2021 Nov 5]. Available from: /pmc/articles/PMC6368897/.
29. Müller-Gärtner HW, Links JM, Prince JL, Bryan RN, McVeigh E, Leal JP, et al. Measurement of radiotracer concentration in brain gray matter using positron emission tomography: MRI-based correction for partial volume effects. J Cereb Blood Flow Metab. 1992;12:571–83 SAGE Publications Sage UK: London, England.
30. Buschke H. Selective reminding for analysis of memory and learning. J Verbal Learn Verbal Behav. 1973;12:543–50 Academic Press.
31. Rosseel Y. Lavaan: An R package for structural equation modeling. J Stat Softw. 2012;48:1–36 American Statistical Association.
32. van Buuren S, Groothuis-Oudshoorn K. Mice: multivariate imputation by chained equations in R. J Stat Softw. 2011;45:1–67.

33. Hong S, Prokopenko D, Dobricic V, Kilpert F, Bos I, Vos SJB, et al. Genome-wide association study of Alzheimer's disease CSF biomarkers in the EMIF-AD Multimodal Biomarker Discovery dataset. Transl Psychiatry. 2020;10:1–12 Nature Publishing Group.
34. Marees AT, de Kluiver H, Stringer S, Vorspan F, Curis E, Marie-Claire C, et al. A tutorial on conducting genome-wide association studies: quality control and statistical analysis. Int J Methods Psychiatr Res. 2018;27:e1608 Wiley.
35. 1000 Genomes Project Consortium, Auton A, Brooks LD, Durbin RM, Garrison EP, Kang HM, Korbel JO, Marchini JL, McCarthy S, McVean GA, Abecasis GR. A global reference for human genetic variation. Nature. 2015;526(7571):68–74. https://doi.org/10.1038/nature15393.
36. Das S, Forer L, Schönherr S, Sidore C, Locke AE, Kwong A, et al. Next-generation genotype imputation service and methods. Nat Genet. 2016;48:1284–7 NIH Public Access.
37. Choi SW, O'Reilly PF. PRSice-2: Polygenic Risk Score software for biobank-scale data. Gigascience. 2019;8:1–6 Oxford University Press.
38. Robin X, Turck N, Hainard A, Tiberti N, Lisacek F, Sanchez JC, et al. pROC: An open-source package for R and S+ to analyze and compare ROC curves. BMC Bioinformatics. 2011;12:1–8 BioMed Central.
39. DeLong ER, DeLong DM, Clarke-Pearson DL. Comparing the areas under two or more correlated receiver operating characteristic curves: a non-parametric approach. Biometrics. 1988;44:837–45.
40. Poline JB, Worsley KJ, Evans AC, Friston KJ. Combining spatial extent and peak intensity to test for activations in functional imaging. Neuroimage. 1997;5:83–96.
41. Schwarz CG, Gunter JL, Lowe VJ, Weigand S, Vemuri P, Senjem ML, et al. A comparison of partial volume correction techniques for measuring change in serial amyloid pet SUVR. J Alzheimers Dis. 2019;67:181–95 IOS Press;[cited 2022 Apr 8]. Available from: /pmc/articles/PMC6398556/.
42. Ge T, Sabuncu MR, Smoller JW, Sperling RA, Mormino EC. Dissociable influences of APOE ε4 and polygenic risk of AD dementia on amyloid and cognition. Neurology. 2018;90:E1605–12 American Academy of Neurology.
43. Leonenko G, Shoai M, Bellou E, Sims R, Williams J, Hardy J, et al. Genetic risk for Alzheimer disease is distinct from genetic risk for amyloid deposition. Ann Neurol. 2019;86:427–35 Wiley-Blackwell.
44. Mishra S, Blazey TM, Holtzman DM, Cruchaga C, Su Y, Morris JC, et al. Longitudinal brain imaging in preclinical Alzheimer disease: impact of APOE ϵ4 genotype. Brain. 2018;141:1828–39 Oxford University Press.
45. Sojkova J, Goh J, Bilgel M, Landman B, Yang X, Zhou Y, et al. Voxel-wise relationships between distribution volume ratio and cerebral blood flow: implications for analysis of β-amyloid images. J Nucl Med. 2015;56:1042 NIH Public Access; [cited 2022 Jul 11]. Available from: https://www.ncbi.nlm.nih.gov/pmc/articles/PMC5367770/.
46. Heeman F, Yaqub M, Lopes Alves I, Heurling K, Bullich S, Gispert JD, et al. Simulating the effect of cerebral blood flow changes on regional quantification of [18F]flutemetamol and [18F]florbetaben studies. J Cereb Blood Flow Metab. 2021;41:579 SAGE Publications; [cited 2022 Jul 11]. Available from: https://www.ncbi.nlm.nih.gov/pmc/articles/PMC7907983/.

Publisher's Note